

Formation of Sodium Bismuth Titanate—Barium Titanate during Solid State Synthesis

Dong Hou,¹ Elena Aksel,^{2,3} Chris M. Fancher,¹ Tedi-Marie Usher,¹ Takuya Hoshina,² Hiroaki Takeda,² Takaaki Tsurumi,² and Jacob L. Jones^{1,a)}

¹*Department of Materials Science and Engineering, North Carolina State University, Raleigh, NC, 27695, USA.*

²*Nano-Phononics Lab., Graduate School of Science and Engineering, Tokyo Institute of Technology, Meguro, Tokyo 152-8552, Japan*

³*SCHOTT AG, Hattenberg Straße 10, 55122 Mainz, Germany*

Abstract

Phase formation of sodium bismuth titanate ($\text{Na}_{0.5}\text{Bi}_{0.5}\text{TiO}_3$ or NBT) and its solid solution with barium titanate (BaTiO_3 or BT) during the calcination process is studied using *in situ* high-temperature diffraction. The reactant powders were mixed and heated to 1000°C, while X-ray diffraction (XRD) patterns were recorded continuously. Phase evolutions from starting materials to final perovskite products are observed, and different transient phases are identified. The formation mechanism of NBT and NBT-*x*BT perovskite structures is discussed, and a reaction sequence is suggested based on the observations. The *in situ* study leads to a new processing approach, which is the use of nano- TiO_2 , and gives insights to the particle size effect for solid-state synthesis products. It was found that the use of nano- TiO_2 as reactant powder accelerates the synthesis process, decreases the formation of transient phases, and helps to obtain phase-pure products using a lower thermal budget.

^a Author to whom correspondence should be addressed. Electronic mail: jacobjones@ncsu.edu

Introduction

NBT is one of the leading candidates currently under investigation as a lead-free alternative to the commonly used lead zirconate titanate (PZT) based materials.^{1,2} Due to the low piezoelectric constant and high coercive field of NBT, it is often investigated in solid solution with other ferroelectric materials.³ One such emerging system that has received significant attention in recent literature is the solid solution of NBT with the classic ferroelectric material BaTiO₃, often referred to as NBT-*x*BT. The improved piezoelectric properties reported for this material system make it a viable alternative for certain applications in which PZT is currently utilized.^{4,5} In order to broaden the application range of NBT-*x*BT and make it as versatile as PZT, a better understanding of the underlying formation mechanism and various factors that affect the properties of NBT-*x*BT is necessary and critical.

In situ high-temperature XRD is applied in the present work instead of *ex situ* characterization methods. Nowadays, revolutionary improvements in laboratory powder diffraction systems enable studies of various material systems under applied stimulus (e.g. temperature, atmosphere, pressure, and electric field), which provides valuable structural information of structure-property relationships, changes in structures, and phase evolution with applied stimuli.^{6,7} Even though *ex situ* methods can offer less noisy XRD patterns due to higher sampling statistics and longer counting time, traditional quenching methods used in *ex situ* methods limit the ability to capture phase evolution that happens in real time. To better understand the formation mechanism and phase evolution of NBT and NBT-*x*BT during solid state synthesis, *in situ* XRD patterns were obtained and investigated.

Experimental

Oxide powders of Bi_2O_3 , TiO_2 , Na_2CO_3 , and BaCO_3 (purity > 99.5%, Wako Pure Chemical Industries) were combined in stoichiometric amounts to obtain various compositions across the NBT-*x*BT phase diagram. The compositions examined in present work were NBT, 0.94NBT-0.06BT (NBT-6BT), 0.91NBT-0.09BT (NBT-9BT), and 0.87NBT-0.13BT (NBT-13BT). For each composition, a second set of reactant mixtures was prepared using nanocrystalline TiO_2 (30 nm, 99.9% purity, Showa Denko K. K.). All the mixed powders were ball milled in ethanol with 5 mm diameter yttria-stabilized zirconia milling media for 24 hours. After drying, the powders were ground and sieved through a 200 μm sieve. Thermogravimetric analysis (TGA) was performed on the prepared powders by using a conventional TGA from TA instruments, with a temperature range of 25°C to 950°C and a heating rate of 10°C/min.

In situ powder diffraction patterns were measured on a PANalytical Empyrean diffractometer using Cu K-alpha radiation with a average wavelength of 0.1542 nm, and with a PIXcel^{1D} Detection System and a HTK 1200N high-temperature oven-chamber. The HTK 1200N heating stage is factory-mounted onto a z-axis, which is adjustable for sample height compensation. Spinning of the sample improves the statistics of the measurement by bringing additional particles into the diffraction condition. The prepared powders were loaded into an alumina sample holder with an inner diameter of 16 mm and a depth of 0.4 mm. A heating rate of 5°C/min was used to heat the samples from room temperature continuously to a maximum temperature of 1000°C, followed by holding at 1000°C for 2 hours and then cooled down to room temperature with a cooling rate of 5°C/min. Diffraction patterns with a 2θ range of 15° to 90° were acquired continuously during heating, holding, and cooling periods. Each individual

pattern was measured for 2 mins, which represents a temperature range of 10°C in the heating and cooling process.

Results and Discussion

I. Calcination Profile

A 3-D shaded surface plot of the diffraction patterns measured during the *in situ* calcination of NBT-6BT is shown in Fig. 1 with intensity on a log scale. The bottom diffraction pattern in this figure represents the reactant mixtures at room temperature, while the top pattern is that of the calcination product at 1000°C. Fig. 1 reveals a great deal of information about the behavior of the starting materials, transient phases, and final products during the calcination process. A compilation of the calcination profiles of all of the different compositions is shown in Fig. S1.1-S1.8 in the supplemental information.

By matching the Bragg peaks of the XRD pattern at room temperature with the International Center for Diffraction Data (ICDD) database, the phases of starting materials were identified as following:

- γ -Na₂CO₃ with a monoclinic *C2/m* structure (Space group #12, ICDD reference code: 01-075-6816)
- TiO₂, with a tetragonal *I4₁/amd* structure (Space group #141, ICDD reference code: 04-014-5764)
- Bi₂O₃, with a monoclinic *P2₁/c* structure (Space group #14, ICDD reference code: 04-003-2034)
- BaCO₃, with an orthorhombic *Pmcn* structure (Space group #62, ICDD reference code: 04-015-3221)

The diffraction pattern of NBT-6BT at room temperature before calcination was extracted from Fig. 1, and re-plotted in Fig. 2(a), and those reactant powder phases were noted below the pattern for a better reference.

With increasing temperature, several peak changes from the starting materials are notable in the 3-D surface plot Fig. 1. To better present the peaks described below, a magnified view of 2θ from 23.5° to 34.0° can be found in Fig. S2 in the supplemental information. Peaks of γ - Na_2CO_3 disappear above 350°C , (e.g. the peak at $2\theta \approx 30.1^\circ$ belonging to (002) plane of γ - Na_2CO_3), suggesting the complete reaction of this phase. The TiO_2 phase was fully reacted above 550°C , indicated by (101) peak at $2\theta \approx 25.3^\circ$, which has the highest intensity in the tetragonal TiO_2 pattern. The Bi_2O_3 phase had reacted by 700°C . The majority of the peaks observed in the room temperature XRD pattern belong to Bi_2O_3 due to the higher atomic scattering factor of Bi and the structure of Bi_2O_3 . Additionally, the positions of different peaks of Bi_2O_3 shift with varying magnitudes during heating due to anisotropic thermal expansion. For example, the different behaviors of (121)/($\bar{1}22$) peak and (200) peak suggests different interplanar spacing expansions under the same temperature increment. Similar behavior is observed across the whole 2θ ranges in Bi_2O_3 , which indicates significant lattice changes of Bi_2O_3 during heating. The BaCO_3 phase disappeared at 780°C , indicated by (111) peak at $2\theta \approx 23.9^\circ$. It is important to note that the temperature at which BaCO_3 fully reacted in our experiment is lower than the thermodynamic equilibrium temperature for direct decomposition of BaCO_3 (which is normally $> 820^\circ\text{C}$)⁸, suggesting a direct solid–solid reaction between BaCO_3 with other reactants.^{8–10}

As shown in Fig. 1 and Fig. S1.1-S1.8, the perovskite structures began to form at 600° , which agrees well with TG-DTA analysis of NBT and NBT-based materials.^{11, 12} The diffraction pattern at 750°C was extracted and re-plotted in Fig. 2(a) to show the formed cubic perovskite

phase. Moreover, addition of BaCO₃ does not change the perovskite formation temperature. After cooling, the final products exist as perovskite NBT or the NBT-*x*BT solid solution.

II. Formation Mechanism

Selected Bragg reflections from the calcination profile of NBT-6BT are presented in Fig. 3(a)-(e) to show more details of the phase evolution; profiles for other compositions can be found in Fig. S3.1-S3.8 in the supplemental information. The *in situ* XRD data of NBT-*x*BT in the present work agrees with the previous observation of NBT by Aksel *et al.*¹³ Similar to Aksel *et al.*, we examined the evolution of the Bragg peaks from the starting mixtures to the final perovskite phases of NBT-*x*BT, and classified the evolution of these peaks into two types: discontinuous type (perovskite peaks form discontinuously from the reactant peaks, e.g. (100) peak in Fig. 3(a)) and continuous type (perovskite peaks form continuously from the reactant peaks, e.g. the (111), (002), and (2 $\bar{1}$ 1) in Fig. 3(c)-(f)). By peak identification, we confirmed that these reactant peaks belongs to Bi₂O₃ phase. Therefore, the continuous transition between the reactant and perovskite peaks suggests a particle conversion mechanism, proposed by Aksel *et al.*, that Bi₂O₃ may act as a host for a diffusion-dependent conversion process during the development of NBT and NBT-*x*BT perovskite structure. Aksel *et al.* also studied the structure relation of Bi₂O₃ and NBT perovskite, and found the similarity in the orientation of the planes in the NBT and Bi₂O₃ phases for the continuous type peaks. This observation furthermore supports the mechanism that appropriate concentrations of other necessary constituent elements incorporate into Bi₂O₃ and this structure transforms into the perovskite structure. A detailed description of particle conversion mechanism can be found in Ref. 13.

In addition, Aksel *et al.* stated the perovskite (110) peak, located in the 2θ range of 32.0° - 34.0° , belongs to discontinuous type. However, in our observations, the peak at $2\theta \approx 32.5^\circ$, which belongs to the Bi_2O_3 ($2\bar{1}1$) plane, transforms to the perovskite (110) peak. A figure describing the similarity in the orientation of the perovskite (110) and the Bi_2O_3 ($2\bar{1}1$) can be found in Fig. S4 in the supplemental information. The absence of the Bi_2O_3 ($2\bar{1}1$) peak in the prior study might result from the limited resolution of the X-ray diffractometer used.

It is important to note that the particle conversion mechanism in formation of NBT-*x*BT is different from the well-studied formation mechanism of BaTiO_3 perovskite. Two main reaction stages during the formation of BaTiO_3 were confirmed by various studies.^{8, 10, 14–18} The first step is dominated by nucleation and growth of BaTiO_3 at the $\text{TiO}_2/\text{BaCO}_3$ contact points and at the TiO_2 surface. Rapid formation of a BaTiO_3 layer occurs at the surface of TiO_2 due to surface diffusion of BaCO_3 . The second step occurs by diffusion of Ba^{2+} and O^{2-} ions from BaCO_3 to TiO_2 core through the BaTiO_3 perovskite layer, forming a core-shell structure during formation. Growth of this BaTiO_3 shell happens until consumption of the TiO_2 core. Unlike the formation of NBT-*x*BT, no continuous peak transition from reactants to perovskite were observed by *in situ* diffraction studies in BaTiO_3 , further supporting that the formation of BaTiO_3 originates from reactions at the interface, instead of the gradual conversion from a structural host to final product.

III. Transient Phases during Synthesis

Some peaks, which do not belong to either the reactant powders or final products, were also observed in specific 2θ and temperature ranges. Fig. 4 shows an example of those transient peaks which occurred during the calcination in the 2θ range of 28.0° - 32.0° . These peaks were

classified into 3 different categories based on different behaviors as a function of temperature or composition. The ICDD was used to identify phases that include Bi, Ba, Na, Ti, and O, and might contribute to these peaks. The phases identified from the ICDD were cross-referenced against the observed transient peaks, and three phases were determined to be a good match: Type 1-BaTiO₃, Type 2-Bi₄Ti₃O₁₂, and Type 3-Ba₂TiO₄, which are generically referred to at the top of Fig. 4. A diffraction pattern of NBT-6BT at 750°C is shown in Fig. 2(b), and those identified phases are marked below the pattern. The following paragraphs discuss each type of transient peaks in details.

The peak at $2\theta \approx 31.5^\circ$ (Type 1 in Fig. 4) is the second most intense peak above 650°C, besides the perovskite final product peak at $2\theta \approx 32^\circ$. This peak can only be observed in NBT-*x*BT compositions, and is not present in NBT. Also, intensity of this peak increases with increasing BT concentration. At the end of the heating steps, this peak remains in all of the Ba-containing compositions, but disappears after the holding period of 2 hours at 1000°C, as shown in Fig. S5 in the supplemental information. There are additional peaks (e.g. at $2\theta \approx 38.6^\circ$, 45.5° , and 56.0°) which are also near to the perovskite peaks for the NBT-*x*BT final product. The positions of these peaks indicate the presence of another perovskite-like phase. By phase identification using the ICDD database, the most reasonable transient phase that contributes to those peaks is BaTiO₃, with a cubic $Pm\bar{3}m$ structure (ICDD reference code: 04-013-6212). The formation of BaTiO₃ is likely a direct result of increased interaction between TiO₂ and BaCO₃ particles due to inhomogeneous local distribution. Additionally, the formation of BaTiO₃, which is closely related to the perovskite NBT and NBT-*x*BT, can presumably lower the energy barrier for the final conversion. It appears that a portion of the reactants firstly form BaTiO₃, which then incorporates into the major NBT-*x*BT phase during the hold at 1000°C.

The peak at $2\theta \approx 30.0^\circ$ (Type 2 in Fig. 4) is obvious in NBT and NBT-6BT samples. This peak only exists from 600°C to 800°C , which is different from the behavior of BaTiO_3 peaks. The phase identification result from the ICDD suggests this peak is the strongest reflection of $\text{Bi}_4\text{Ti}_3\text{O}_{12}$ with an orthorhombic *B2eb* structure (ICDD reference code: 04-009-5135). $\text{Bi}_4\text{Ti}_3\text{O}_{12}$ has also been reported as a secondary phase by other studies on similar perovskite systems. For example, Xu *et al.* reported an intermediate phase of $\text{Bi}_4\text{Ti}_3\text{O}_{12}$ in NBT in the 500°C to 550°C range using the citrate synthesis method;¹⁹ Morozov *et al.* suggested the formation of $\text{Bi}_4\text{Ti}_3\text{O}_{12}$ from Bi_2O_3 and TiO_2 becomes noticeable at temperatures above 600°C ;²⁰ Aksel *et al.* reported $\text{Bi}_4\text{Ti}_3\text{O}_{12}$ secondary phase in the 500°C to 650°C temperature range using *in situ* XRD method.¹³ The various observed temperature ranges of $\text{Bi}_4\text{Ti}_3\text{O}_{12}$ might result from different starting powders, processing methods, and/or different heating rates. The previous studies, together with this current work, strongly suggest the existence of a secondary reaction and a transient $\text{Bi}_4\text{Ti}_3\text{O}_{12}$ phase during the processing of NBT and NBT-*x*BT. The relative intensity of $\text{Bi}_4\text{Ti}_3\text{O}_{12}$ decreased with increasing BT content, likely because there are less Bi precursors and Ba suppresses the reaction between Bi_2O_3 and TiO_2 that occurs at particles' interface.

The peak at $2\theta \approx 29.0^\circ$ (Type 3 in Fig. 4) is distinguishable in NBT-*x*BT (Fig. 4(b)-(d)), while invisible in NBT. This peak is firstly observed at 650°C and disappears above 850°C . With increasing BT concentration, the intensity of the Type 3 peak increases, suggesting this phase is Ba-dependent. This peak also displays different behaviors in samples that are prepared with different types of TiO_2 (e.g. Fig. 4(d) and (f)), suggesting this phase is also Ti-dependent. Prior literature reported the co-existence of Ba_2TiO_4 in the processing of BaTiO_3 or BaTiO_3 based materials,^{8, 21–24} and this phase agrees with our phase identification result (monoclinic *P2₁/n*, ICDD reference code: 00-035-0813). Alternately, Triamnak *et al.* previously observed the

BaBiO₃ phase, which can also fit the given peak at $2\theta \approx 29.0^\circ$.²³ However, BaBiO₃ is a less likely candidate due to the lack of Ti in the material. Therefore, the most likely phase corresponding to the Type 3 peak is Ba₂TiO₄. The formation of Ba₂TiO₄ may be due to the interaction between BaCO₃ and TiO₂.

Formation of all of the above transient phases occurred discontinuously from the reactant peaks, suggesting the transient phases form via a nucleation and growth mechanism, instead of the particle conversion mechanism that occurs in the formation of NBT-*x*BT. Transient phases finally convert to the NBT or NBT-*x*BT perovskite phase after heat treatments.

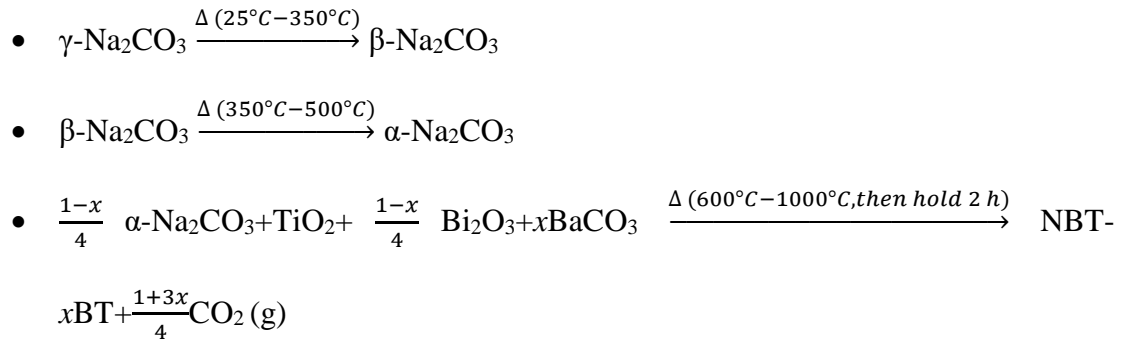
IV. Transformation of Na₂CO₃

In addition to the transient phases, an interesting phase transformation of Na₂CO₃ was also observed in the present work. There is a notable feature in Fig. 1 and Fig. S1.1-S1.8; a low intensity peak which starts at $2\theta \approx 30.1^\circ$ and shifts to $2\theta \approx 28.0^\circ$ at a rapid rate in the temperature range of 150°C to 450°C. A magnified view for this specific area can be seen in Fig. 5. The Bragg peak at this 2θ position can be indexed as Na₂CO₃. At atmospheric pressure, Na₂CO₃ exists as four polymorphs (α , β , γ , and δ), and continuous phase transitions between the α , β and γ phases at various temperatures were reported using infrared absorption and neutron powder diffraction studies.²⁵⁻²⁷ At room temperature, Na₂CO₃ is present in its monoclinic γ -phase and it transforms to the monoclinic β -phase with heating. The rapid shift in this observed Na₂CO₃ peak is attributed to the higher rate of thermal expansion in β -Na₂CO₃.²⁷ Based on an infrared absorption study by Harris *et al.*,²⁶ the transition of γ -phase to β -phase finishes at 346°C, which agrees well with our *in situ* XRD data that shows the disappearance of γ -phase (002) peak ($2\theta \approx 30.1^\circ$) at $\approx 350^\circ\text{C}$. Additionally, they reported that transition of β -Na₂CO₃ to α -Na₂CO₃ starts

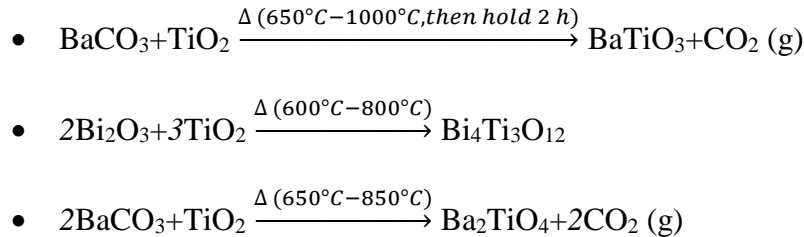
at 346°C and ends at 490°C, which also matches with our experimental data that shows β - Na_2CO_3 disappeared at $\approx 500^\circ\text{C}$. For temperatures above 500°C and below 600°C, Na_2CO_3 exists in the α -phase, and the Bragg peaks of α - Na_2CO_3 are covered by stronger Bi_2O_3 peaks in our study.

In summary, according to the present *in situ* XRD data, the reaction processes that occur during the phase formation of NBT- x BT can be represented by the following steps:

(Primary phase sequence)



(Secondary phase sequence)



TGA results in Fig. S6 in the supplemental information agrees well with the conclusions drawn from *in situ* XRD. As shown in Fig. S6(a), the weight loss steps at 385°C might correspond to the transition of β - Na_2CO_3 to α phase, and the partial decomposition of Na_2CO_3 ; the significant weight drop at 623°C contributes from the reaction between raw powders and the formation of NBT- x BT; the small weight loss at 820°C comes from the formation of secondary phases.

V. Nano Particles Effects

Based on the particle conversion mechanism, we hypothesize that the particle sizes of the starting materials will affect the phase sequence: if the size of TiO_2 particles is reduced, the incorporation of those particles into the Bi_2O_3 host can be promoted, and therefore the conversion process will be accelerated. The reason that nano crystalline Bi_2O_3 was not varied in this study is that decreasing the host particle size (i.e., the use of nano- Bi_2O_3) would result in smaller grain sizes of the final products. In contrast, the present study focuses on accelerating the reaction by varying the size of the particles consumed in the reaction. Grain size effect on the final products' electrical properties has been reported on different systems, e.g. Hao *et al.* states decreasing grain size leads to weaker piezoelectric properties and lower resistance to thermal depoling in $(\text{Ba}_x\text{Ca}_{1-x})(\text{Zr}_y\text{Ti}_{1-y})\text{O}_3$;²⁸ McCauley *et al.* studied the intrinsic size effects of BaTiO_3 on dielectric constant, loss, and transition temperature, and found ferroelectric transition cannot be supported below a critical grain size.²⁹ By using nano- TiO_2 , potential changes in grain size effect can be mitigated since the host particle size remains the same. Decreasing the size of the TiO_2 particles can also affect the phase transition. Binder reported both first- and second-order transitions get smeared and shifted due to particle size effect based on Monte Carlo simulations.³⁰ Various studies have proved that decreasing particle size can lower the calcination temperature, suppress secondary phases, and affect the performance of the materials.^{17, 31–34} Therefore we expect fewer secondary, transient phases and lower phase formation temperature in this material system by using nano- TiO_2 . To better understand the mechanism, and to prove our hypothesis, nano- TiO_2 based reactant mixtures for NBT and NBT- x BT were prepared, and their calcinations were investigated *in situ*.

The particle size of the reactant TiO_2 powder has several effects on the calcination process of NBT and NBT- x BT. The *in situ* calcination profiles of nano- TiO_2 based compositions can be found in Fig. S1.5-S1.8 and Fig. S3.5-S3.8 in the supplemental information. Diffraction patterns within a limited 2θ range to emphasize the transient phases in nano- TiO_2 based compositions are given in Fig. 4(e)-(h). The use of nano- TiO_2 shifted the temperature of the perovskite formation down to 500°C , in comparison to the formation temperature of 600°C in compositions prepared using normal commercial TiO_2 , confirming our hypothesis that the conversion process will be accelerated. Along with the perovskite final product, the transient phases also shifted to a lower temperature ranges by using the nano- TiO_2 . For example, the $\text{Bi}_4\text{Ti}_3\text{O}_{12}$ phase is firstly observed at 550°C and disappears at 750°C in Fig. 4(e), showing a 50°C decrease from the normal- TiO_2 based compositions; the BaTiO_3 phase is no longer present at the end of the heating cycle, suggesting a phase-pure NBT- x BT is obtained without holding at 1000°C for more thermal input. The difference of TGA results between normal- TiO_2 based and nano- TiO_2 based reactant powders strengthens our arguments. For example, as shown in Fig. S6(a) and (b), the derivative weight peak at 623°C , suggesting the formation of NBT- x BT, dropped to 552°C by using nano- TiO_2 method, while the derivative weight peak at 820°C , showing the formation of secondary phases, dropped to 700°C by using nano- TiO_2 . Additionally, the relative intensity of the transient peaks is reduced for the compositions prepared with nano- TiO_2 , some of the transient peaks shown in normal- TiO_2 based compositions cannot even be observed, confirming our hypothesis that less secondary phases form in the system. The lower formation temperature and weaker intensity of transient phases likely results from the greater specific surface area of nano- TiO_2 . The area where the reactants can interact is increased in nano- TiO_2 particles, which can allow for more contact area through which TiO_2 can incorporate

into Bi_2O_3 to form the final product or react with other particles to form transient phases. High surface area also provides higher stored energy for solid-state synthesis.³⁵ Therefore, the reaction dynamics appear to be accelerated by using nano- TiO_2 , and NBT- x BT products with higher purity can be achieved with a lower calcination temperature and smaller thermal budget.

Conclusion

In summary, an *in situ* XRD study of the phase evolution behaviors of NBT and NBT- x BT during solid-state synthesis was reported. Based on our observations, the formation of NBT and NBT- x BT perovskite products can be explained using the particle conversion mechanism. By examining the *in situ* XRD patterns of different compositions, it is clear that intermediate phases strongly influence the phase development of NBT and NBT- x BT, and the addition of BaCO_3 dramatically changes the phases present, reaction sequence, and temperature ranges of those intermediate phases formed during synthesis. The formation of the perovskite final products is a complex reaction sequence with multiple steps, several of which were described in this work. Studying the reactions *in situ* helps to explain known phenomena in the NBT- x BT system, and is useful in improving processing route. The use of nano- TiO_2 as reactant powder accelerates the synthesis process, decreases transient phases, and offers potential for obtaining high purity multicomponent products with lower processing temperatures, in which final products with tailored and predictable properties could be prepared.

Acknowledgments

This work was performed in part at the Analytical Instrumentation Facility (AIF) at North Carolina State University, which is supported by the State of North Carolina and the National

Science Foundation (award number ECCS-1542015). The AIF is a member of the North Carolina Research Triangle Nanotechnology Network (RTNN), a site in the National Nanotechnology Coordinated Infrastructure (NNCI). D.H. thanks financial support of China Scholarship Council. E.A. acknowledges support from the Japan Society for the Promotion of Science. The authors thank Hanhan Zhou, Emily Lichtenberger and Birgit Andersen for the thermogravimetric measurements.

References

- 1 G.A. Smolenskii, V.A. Isupov, A.I. Agranovskaya, and N.N. Krainik, "NEW FERROELECTRICS OF COMPLEX COMPOSITION. 4.," *Sov. Physics-Solid State*, **2** [11] 2651–2654 (1961).
- 2 J. Rödel, W. Jo, K.T.P. Seifert, E. Anton, T. Granzow, and D. Damjanovic, "Perspective on the Development of Lead-free Piezoceramics," *J. Am. Ceram. Soc.*, **92** [6] 1153–1177 (2009).
- 3 Y. Hiruma, H. Nagata, and T. Takenaka, "Thermal depoling process and piezoelectric properties of bismuth sodium titanate ceramics," *J. Appl. Phys.*, **105** [8] 4112 (2009).
- 4 T. Takenaka, K. Maruyama, and K. Sakata, "(Bi_{1/2}Na_{1/2}) TiO₃-BaTiO₃ system for lead-free piezoelectric ceramics," *Jpn. J. Appl. Phys.*, **30** [9S] 2236 (1991).
- 5 Y. Hiruma, K. Yoshii, H. Nagata, and T. Takenaka, "Investigation of phase transition temperatures on (Bi_{1/2}Na_{1/2}) TiO₃-(Bi_{1/2}K_{1/2}) TiO₃ and (Bi_{1/2}Na_{1/2}) TiO₃-BaTiO₃ lead-free piezoelectric ceramics by electrical measurements," *Ferroelectrics*, **346** [1] 114–119 (2007).
- 6 S.T. Mixture, "In situ X-ray diffraction studies of electroceramics," *J. electroceramics*, **16** [2] 167–178 (2006).
- 7 G. Esteves, C.M. Fancher, and J.L. Jones, "In situ characterization of polycrystalline ferroelectrics using x-ray and neutron diffraction," *J. Mater. Res.*, **30** [03] 340–356 (2015).
- 8 M.T. Buscaglia, M. Bassoli, V. Buscaglia, and R. Vormberg, "Solid-state synthesis of nanocrystalline BaTiO₃: Reaction kinetics and powder properties," *J. Am. Ceram. Soc.*, **91** [9] 2862–2869 (2008).
- 9 T. Zaremba, "Thermoanalytical study of the synthesis of Na_{0.5}Bi_{0.5}TiO₃ ferroelectric," *J. Therm. Anal. Calorim.*, **92** [2] 583–587 (2008).
- 10 M.T. Buscaglia, M. Bassoli, V. Buscaglia, and R. Alessio, "Solid-State Synthesis of Ultrafine BaTiO₃ Powders from Nanocrystalline BaCO₃ and TiO₂," *J. Am. Ceram. Soc.*, **88** [9] 2374–2379 (2005).
- 11 W. Ge, H. Liu, X. Zhao, X. Pan, T. He, D. Lin, H. Xu, and H. Luo, "Growth and characterization of Na_{0.5}Bi_{0.5}TiO₃-BaTiO₃ lead-free piezoelectric crystal by the TSSG method," *J. Alloys Compd.*, **456** [1-2] 503–507 (2008).
- 12 T. Kainz, M. Naderer, D. Schütz, O. Fruhwirth, F.A. Mautner, and K. Reichmann, "Solid state synthesis and sintering of solid solutions of BNT-xBKT," *J. Eur. Ceram. Soc.*, **34** [15] 3685–3697 (2014).
- 13 E. Aksel and J.L. Jones, "Phase Formation of Sodium Bismuth Titanate Perovskite During Solid State Processing," *J. Am. Ceram. Soc.*, **93** [10] 3012–3016 (2010).
- 14 S.S. Ryu and D.H. Yoon, "Solid-state synthesis of nano-sized BaTiO₃ powder with high tetragonality," *J. Mater. Sci.*, **42** [17] 7093–7099 (2007).
- 15 L.B. Kong, J. Ma, H. Huang, R.F. Zhang, and W.X. Que, "Barium titanate derived from

- mechanochemically activated powders,” *J. Alloys Compd.*, **337** [1-2] 226–230 (2002).
- 16 V. Berbenni, A. Marini, and G. Bruni, “Effect of mechanical milling on solid state formation of BaTiO₃ from BaCO₃-TiO₂ (rutile) mixtures,” *Thermochim. Acta*, **374** [2] 151–158 (2001).
- 17 D.F.K. Hennings, B.S. Schreinemacher, and H. Schreinemacher, “Solid-State Preparation of BaTiO₃ -Based Dielectrics, Using Ultrafine Raw Materials,” *J. Am. Ceram. Soc.*, **84** [12] 2777–2782 (2001).
- 18 F. Bondioli, A. Bonamartini Corradi, A.M. Ferrari, T. Manfredini, and G.C. Pellacani, “Kinetic Study of Conventional Solid-State Synthesis of BaTiO₃ by *in situ* HT-XRD,” *Mater. Sci. Forum*, **278-281** 379–383 (1998).
- 19 Q. Xu, S. Chen, W. Chen, D. Huang, J. Zhou, H. Sun, and Y. Li, “Synthesis of (Na_{0.5}Bi_{0.5})TiO₃ and (Na_{0.5}Bi_{0.5})_{0.92}Ba_{0.08}TiO₃ powders by a citrate method,” *J. Mater. Sci.*, **41** [18] 6146–6149 (2006).
- 20 M.I. Morozov, L.P. Mezentseva, and V. V Gusarov, “Mechanism of formation of Bi₄Ti₃O₁₂,” *Russ. J. Gen. Chem.*, **72** [7] 1038–1040 (2002).
- 21 A. Beauger, J.C. Mutin, and J.C. Niepce, “Synthesis reaction of metatitanate BaTiO₃,” *J. Mater. Sci.*, **18** [10] 3041–3046 (1983).
- 22 W. Chaisan, R. Yimmirun, and S. Ananta, “Effect of vibro-milling time on phase formation and particle size of barium titanate nanopowders,” *Ceram. Int.*, **35** [1] 173–176 (2009).
- 23 N. Triamnak, G.L. Brennecke, H.J. Brown-Shaklee, M.A. Rodriguez, and D.P. Cann, “Phase formation of BaTiO₃-Bi (Zn_{1/2}Ti_{1/2})O₃ perovskite ceramics,” *J. Ceram. Soc. Japan*, **122** [1424] 260–266 (2014).
- 24 S. Lee, C.A. Randall, and Z.K. Liu, “Modified phase diagram for the barium oxide-titanium dioxide system for the ferroelectric barium titanate,” *J. Am. Ceram. Soc.*, **90** [8] 2589–2594 (2007).
- 25 M.J. Harris, M.T. Dove, and K.W. Godfrey, “A single-crystal neutron scattering study of lattice melting in ferroelastic,” *J. Phys. Condens. Matter*, **8** [38] 7073 (1996).
- 26 M.J. Harris and E.K.H. Salje, “The incommensurate phase of sodium carbonate: an infrared absorption study,” *J. Phys. Condens. Matter*, **4** [18] 4399 (1992).
- 27 I.P. Swainson, M.T. Dove, and M.J. Harris, “Neutron powder diffraction study of the ferroelastic phase transition and lattice melting in sodium carbonate, Na₂CO₃,” *J. Phys. Condens. Matter*, **7** [23] 4395 (1995).
- 28 J. Hao, W. Bai, W. Li, and J. Zhai, “Correlation Between the Microstructure and Electrical Properties in High-Performance (Ba_{0.85}Ca_{0.15})(Zr_{0.1}Ti_{0.9})O₃ Lead-Free Piezoelectric Ceramics,” *J. Am. Ceram. Soc.*, **95** [6] 1998–2006 (2012).
- 29 D. McCauley, R.E. Newnham, and C. a. Randall, “Intrinsic Size Effects in a Barium Titanate Glass-Ceramic,” *J. Am. Ceram. Soc.*, **81** [4] 979–987 (1998).

- 30 K. Binder, "Finite size effects on phase transitions," *Ferroelectrics*, **73** [1] 43–67 (1987).
- 31 M.S. Yoon, N.H. Khansur, B.K. Choi, Y.G. Lee, and S.C. Ur, "The effect of nano-sized BNBT on microstructure and dielectric/piezoelectric properties," *Ceram. Int.*, **35** [8] 3027–3036 (2009).
- 32 B. Li, X. Wang, M. Yan, and L. Li, "Preparation and characterization of nano-TiO₂ powder," *Mater. Chem. Phys.*, **78** 184–188 (2002).
- 33 L.. Kong, J. Ma, W. Zhu, and O.. Tan, "Preparation of Bi₄Ti₃O₁₂ ceramics via a high-energy ball milling process," *Mater. Lett.*, **51** [2] 108–114 (2001).
- 34 E. Brzozowski and M.S. Castro, "Lowering the synthesis temperature of high-purity BaTiO₃ powders by modifications in the processing conditions," *Thermochim. Acta*, **398** [1-2] 123–129 (2003).
- 35 S. Bose and A. Banerjee, "Novel Synthesis Route to Make Nanocrystalline Lead Zirconate Titanate Powder," *J. Am. Ceram. Soc.*, **87** [3] 487–489 (2004).

Appendix

FIG. 1. in situ diffraction patterns taken during the heating stage of solid-state synthesis of NBT-6BT.

FIG. 2. Diffraction patterns of the mixed reactant powders of NBT-6BT (a) before calcination, and (b) during calcination at 750°C. Phases of reactant were identified in (a); cubic perovskite phase and transient phases during calcination were noted in (b).

FIG. 3. Selected Bragg reflections from the calcination profile of NBT-6BT. The perovskite peak at the top of each subplot is (100), (110), (111), (002), and ($\bar{2}11$) for (a) to (f), respectively.

FIG. 4. in situ calcination profile in the 2θ range of 28.0°-32.0° for NBT, NBT-6BT, NBT-9BT, NBT-13BT (a to d); and for nano-TiO₂ based compositions of NBT, NBT-6BT, NBT-9BT, NBT-13BT (e to h). (Type 1-BaTiO₃, Type 2-Bi₄Ti₃O₁₂, and Type 3-Ba₂TiO₄)

FIG. 5. in situ calcination profile at selected 2θ range to emphasize the peak changes of Na₂CO₃